Published in final edited form as:
Stem Cells. 2009 October ; 27(10): 2614–2623. doi:10.1002/stem.187.

Direct Evidence of Mesenchymal Stem Cell Tropism for Tumor and Wounding Microenvironments using *In Vivo* Bioluminescence Imaging

Shannon Kidd[1], **Erika Spaeth**[1], **Jennifer L. Dembinski**[2], **Martin Dietrich**[3], **Keri Watson**[1], **Ann Klopp**[4], **Lokesh Battula**[1], **Micheal Weil**[5], **Michael Andreeff**[1], and **Frank C. Marini**[1]

[1]Section of Molecular Hematology and Therapy, Dept of Stem Cell Transplantation and Cellular Therapy, UT-M.D. Anderson Cancer Center, Houston, TX 77030

[4]Dept of Radiation Oncology, UT-M.D. Anderson Cancer Center, Houston, TX 77030

Abstract

Multipotent mesenchymal stromal/stem cells (MSC) have shown potential clinical utility. However, previous assessments of MSC behavior in recipients have relied on visual detection in host tissue following sacrifice, failing to monitor *in vivo* MSC dispersion in a single animal and limiting the number of variables that can be observed concurrently. In this study, we utilized noninvasive, *in vivo* bioluminescent imaging to determine conditions under which MSC selectively engraft in sites of inflammation. MSC modified to express firefly luciferase (MSC-ffLuc) were injected into healthy mice or mice bearing inflammatory insults, and MSC localization was followed with bioluminescent imaging. Inflammatory insults investigated included cutaneous needle-stick and surgical incision wounds, as well as xenogeneic and syngeneic tumors. We also compared tumor models in which MSC were intraveneously or intraperitoneally delivered. Our results demonstrate hMSC-ffLuc systemically delivered to non-tumor bearing animals initially reside in the lungs, then egress to the liver and spleen and decrease in signal over time. However, hMSC in wounded mice engraft and remain detectable only in injured sites. Similarly, in syngeneic and xenogeneic breast carcinoma-bearing mice, bioluminescent detection of systemically delivered MSC revealed persistent, specific co-

*- to whom all correspondences should be addressed: Frank C Marini Ph.D., Stem Cell Transplant and Cellular Therapy/BOX081, M.D. Anderson Cancer Center, 1515 Holcombe Blvd, Houston, TX 77030, 713.794.5644-office, 713.794.4747-FAX, fmarini@mdanderson.org.
[2]Current address, Norwegian Centre for Stem Cell Research, Institute of Microbiology, Rikshospitalet, Forskningsparken, Gaustadalléen, Oslo, Norway.
[3]Current Address-The University of Texas Southwestern Medical Center, Dallas, TX 75390.
[5]Current Address, Department of Environmental and Radiological Health Sciences, Colorado State University, Fort Collins, CO 80523

Author contribution summary: Shannon Kidd: conception and design, collection and assembly of data, data analysis and interpretation, manuscript writing
Erika Spaeth: conception and design, data analysis and interpretation, manuscript writing
Jennifer L. Dembinski: conception and design, collection and assembly of data, data analysis and interpretation
Martin Dietrich: collection and assembly of data, provision of study material
Keri Watson: collection and assembly of data
Ann Klopp: collection and assembly of data
Lokesh Battula: collection and assembly of data
Micheal Weil: provision of study material
Michael Andreeff: conception and design, financial support
Frank C. Marini: conception and design, data analysis and interpretation, financial support, final approval of manuscript

localization with sites of tumor development. This pattern of tropism was also observed in an ovarian tumor model in which MSC were IP injected. In this study we have identified conditions under which MSC tropism and selective engraftment in sites of inflammation can be monitored by bioluminescent imaging over time. Importantly, these consistent findings were independent of tumor type, immunocompetence and route of MSC delivery.

Keywords

Mesenchymal stem cell; tumor tropism; inflammatory microenvironment; bioluminescent imaging

Introduction

Multipotent mesenchymal stromal cells (MSC), also referred to as mesenchymal stem cells, have demonstrated preferential incorporation into sites of tumor development [1, 2], and injury [3-5]. This selective integration has been attributed to the high levels of inflammatory mediators produced in the associated microenvironment [6]. Tissues confronted with acute insults involve states of injury that exhibit an array of inflammatory chemotactic molecules to which MSC respond (reviewed in Spaeth, 2008 [6]). Such states include *i)* hypoxia or ischemia[7-10] a state of reduced oxygen that often parallels and perpetuates inflammation, *ii)* radiation, used as therapy or as a weapon [11-13] *iii)* tumors, which mimic the phenotype of an “unhealed wound” [14] *iv)* and cutaneous cuts or punctures that delineate the conventional definition of inflammation [15]. Exploitation of this MSC tropism offers numerous therapeutic applications for an array of disorders including myocardial infarction [16-18], muscular dystrophy [19], osteogenesis imperfecta [20], spinal cord injury [21], graft-versus-host-disease [22], and cancer [1, 2]. Despite the great therapeutic potential, unanswered questions remain regarding homing, engraftment and safety of the transplanted stem cells [23].

In animal experiments, labeled MSC can be monitored by immunohistochemical staining [11], fluorescent visualization [24], or DNA-PCR [25, 26] to examine the migratory end point of these labeled cells only after the animal has been sacrificed. While sensitive, these methods require the use of numerous animals to be sacrificed at multiple time points and allow the opportunity for sampling limitations to occur when only certain parts of the tissue or organ are harvested and analyzed. To circumvent single time point experiments, we have employed *in vivo* bioluminescent imaging. This method detects visible light produced when cells modified to express reporter enzymes, such as firefly luciferase (ffLuc), react with their specific bioluminescent substrates [27] and allows for non-invasive, serial detection of these cells *in vivo* [28, 29]. Though visible light is limited in depth of tissue penetration, the technique is ideal and cost-effective for imaging small animals such as mice. Additionally, multiple labeled cell populations can be detected in the same animal, affording the use of significantly fewer animals than previous methods. Furthermore, these reporter enzymes are only expressed in viable, metabolically active cells [30]. Bioluminescent imaging has already facilitated the study of tumor growth and response to treatments [31, 32], gene expression in cells [29], the trafficking of lymphocytes *in vivo* [33], and hematopoietic stem cell engraftment in host tissues [34, 35]. This method has also been utilized to image MSC

injected into myocardium [36-38], models of acute kidney injury [39], and in subcutaneously transplanted ceramic cubes [40] and scaffolds [41].

We show herein that bioluminescent imaging can reveal dynamic information detailing the distribution and tropism of MSC in host tissues towards inflammatory tumor and wound microenvironments. We demonstrate the biodistribution of systemically injected hMSC in non tumor-bearing SCID mice, where hMSC initially distribute to the lungs, liver and spleen and then diminish in bioluminescent signal until they are undetectable at 14 days. We then show specific co-localization of injected hMSC in two different cutaneous wounding events. Next, we followed MSC in tumor bearing SCID mice and found selective MSC engraftment at the site(s) of tumor development when MSC were delivered by intraveneous or intraperitoneal administration. Finally, similar results were seen in an immunocompetent, syngeneic Balb/C breast tumor model in which mMSC specifically co-localized with subcutaneously established tumors. Regardless of immunocompetence or route of MSC administration, bioluminescent imaging revealed specific tropism and engraftment of MSC in all tumor and wounding models investigated, indicating MSC could be useful biodetectors of these disease states.

Materials and Methods

Isolation and expansion of human and murine MSC

Human MSC (hMSC) were isolated from the bone marrow of normal individuals undergoing bone marrow harvest for allogeneic bone marrow transplantation following informed consent, according to institutional guidelines under the approved protocol, as described previously [2]. Briefly, mononuclear cells were separated by centrifugation over a Ficoll-Hypaque gradient (Sigma, St. Louis, MO) and suspended in 10 ml of MSC complete medium: alpha-minimum essential medium (α-MEM) containing 20% fetal bovine serum (FBS; Invitrogen, Carlsbad, CA), L-glutamine and penicillin-streptomycin mixture (Gibco/Invitrogen, Carlsbad, CA) and plated in 180 cm^2 dish. After 3 days, the non-adherent cells were removed by washing with phosphate buffered saline (PBS) and monolayers of adherent cells were cultured until they reached confluence. Cells were then trypsinized (0.25% trypsin with 0.1% EDTA) and sub-cultured at densities of 5,000-6,000 cells/cm^2. Cell passages 3 to 4 were used for the experiments.

Murine MSC (mMSC) were isolated as described previously [42]. Briefly, femurs of 2-month-old Balb/C (Harlan Labs, ME) were collected, dissected into small fragment, then placed into a sterile mortar and crushed using a sterile pestle. Whole bone fragments and bone marrow pieces were then placed *in toto* into 10 ml MSC complete medium and plated in 180 cm^2 dish. After five days the plate was washed to remove non-adherent cells After two complete washings adherent cells were retrieved by trypsinization and immunodepleted of granulo-monocytic cells using a biotinylated antibody against CD11b (BD Biosciences, San Jose, CA), and streptavidin-coated microbeads from Miltenyi Biotec (Auburn, CA) according to the manufacturer's instructions. After immunodepletion, the remaining cells were plated in fresh media, and within 3 additional days, fibroblast-like colonies were observed. Medium was changed two to three times a week and cell density was maintained between 2,000 and 6,000cell/cm^2.

To determine the multi-lineage differentiation potential of the human MSC, we subjected passage 3 hMSC to various differentiation media, according to manufacturer recommendations (Miltenyi Biotec, Auburn, CA). Briefly, hMSC were cultured for 3 weeks in NH AdipoDiff, NH OsteoDiff, or ChondroDiff media with media changes ever 3 days. Adipocytes were then stained with Oil Red O (Sigma), and osteoblasts were stained for calcium with Alizarin Red S. For chondrogenic detection, hMSC pellets were sectioned and stained with Alcian Blue. ffLuc labeled MSC were also assayed for adiopgenic, osteogenic and chondrogenic potentials.

Cell Culture

Human MDA-MB-231 breast cancer cells (a generous gift from Dr. I. Fidler, M. D. Anderson Cancer Center, Houston, TX), were maintained in α-MEM containing 10% FBS, sodium pyruvate, nonessential amino acids, L-glutamine, vitamin solution (Life Technologies, Grand Island, NY), and penicillin–streptomycin. Human ovarian cancer HEY cells and murine breast carcinoma 4T1 cells were obtained from American Type Culture Collection (ATCC, Manassas, VA) and cultured in Roswell Park Memorial Institute medium (RPMI-1640) supplemented with 10% FCS and penicillin–streptomycin. Murine 4T1 cells were stably transduced with a lentivirus expressing renilla luciferase (4T1-rLuc), as described previously [42].

Flow Cytometry

MSC were harvested with 0.25% trypsin-EDTA and resuspended in phosphate buffered saline (PBS) supplemented with 2% FBS. Approximately 1×10^6 cells were stained with 1μg of antibody for 30 minutes at 4°C, and then analyzed on a FACSCaliber (Becton-Dickson, San Jose, CA). Human antibodies used included CD105, CD90, CD140b, CD73, CD166, CD44, CD146, CD31 and CD34 (BD Bioscience, San Jose, CA). Antibodies specific for mouse antigens included Sca-1, CD106, CD140b, CD44, CD31, CD11b and CD45 (eBiosciences, San Diego, CA).

Adenoviral vector and MSC transduction

A recombinant adenoviral (Ad) vector expressing firefly luciferase (ffLuc), possessing an RGD-modified fiber (AdLuc-F/RGD) was prepared, purified, and titered as described previously [43]. Human MSC were incubated with AdLuc-F/RGD at 3,000 viral particles per cell (vp/cell) (based on OD reading) for 4 hours, while Balb/C and C57Bl/6 MSC were incubated with AdLuc-F/RGD at 5,000 vp/cells for 6 hours in serum-free medium. After incubation serum containing media was added to the culture. Transduction efficiency was routinely above 95% in both hMSC and mMSC, as previously reported [43]. MSC were assessed for luciferase expression by plating 5×10^4 transduced MSC into 24 well plates and adding 1μl of D-Luciferin (40mg/ml stock) (Caliper Life Sciences [Xenogen], Hopkinton, MA) into 2ml culture medium. 30 sec later cells were placed into the imager for detection. Using this multiplicity of infection (MOI) protocol, we routinely detected >500 copies of Ad-delivered ffLuc transcript/MSC by qRT-PCR, and bioluminescence could be detected for up to 30 days (data not shown). A single transfection was performed at each time point to provide all animals in the same experiment with the same source of donor MSC.

Animals

Female Balb/C and severe combined immune disorder (SCID)/CB-17 mice were purchased from Jackson Lab (Bar Harbor ME). Mice were used in accordance with institutional guidelines under the approved protocols.

Subcutaneous detection of MSC *in vivo*

Cell doses ranging from 10 to 300 MSC-ffLuc were injected subcutaneously (SC) in 10μl PBS (n=3). A control animal was injected with PBS alone. Immediately post-injection, hMSC-ffLuc bioluminescence was detected and imaged with the Xenogen IVIS after substrate administration.

MSC administration to non-tumor bearing animals

1×10^6 hMSC-ffLuc suspended in 100μl PBS were injected into the tail vein of SCID mice (n = 5). The mice were imaged for bioluminescence detection to pinpoint hMSC-ffLuc location at 1, 3, 5, 7, and 10 days post MSC injection. Likewise, 1×10^6 mMSC-ffLuc generated from a Balb/C mouse, suspended in 100μl PBS were IV injected via tail vein in syngeneic Balb/C mice (n=5). These mice were imaged 1.5, 2.5, 10, 18, and 24 hours post mMSC-ffLuc injection.

Cutaneous wounding models and MSC administration

Anesthetized SCID mice were shaved and cleaned with sterile alcohol and gauze. A subcutaneous surgical incision (1.25cm) was made on the right side of the abdomen (n=3). This incision was immediately sutured shut with 5 stitches, and the mouse was isolated in a private cage. Three days post-surgery, the mice were injected via tail vein with 2.5×10^5 hMSC-ffLuc. The tail vein puncture wounding experiments were done on mice receiving 3 separate injections using a 27 gauge needle along the lateral tail veins during the injection of 2.5×10^5 ffLuc-MSC (n=5). All wounded mice were imaged over a period of 2 weeks, at which time point they were sacrificed.

Tumor models and MSC administration

Xenograft tumors: 5×10^5 MDA-MB-231 cells in 100μl of PBS were administered IV via the tail vein of SCID mice and allowed to seed the lungs (n=5). After 10 days, 1×10^6 ffLuc labeled hMSC (hMSC-ffLuc) were IV injected in 100μl PBS. hMSC-ffLuc localization was tracked by bioluminescence imaging twice per week until sacrifice of the animals at Day 29. 5×10^5 HEY ovarian carcinoma cells were suspended in 1 ml of PBS and intraperitoneally (IP) injected into SCID mice (n=3). 15 days post-tumor injection, 1×10^6 hMSC-ffLuc were IP injected in 100μl PBS, and these cells were monitored 3 times per week for 2 weeks, at which time point these animals were sacrificed. **Syngeneic tumors:** 2.5×10^5 Balb/C derived murine 4T1 breast carcinoma cells were subcutaneously injected into the hind limbs of Balb/C mice. After 10 days of tumor establishment, 1×10^6 mMSC-ffLuc were IV injected as described previously and followed by imaging 2 times a week until sacrifice at 12 days. See supplemental table 1 for a table detailing the experimental design of the tumor models. In all experiments, mice were allowed to recover for 1hr before being placed into group cages after injection.

Bioluminescent imaging

In vivo optical imaging was performed with a Xenogen IVIS bioluminescence/fluorescence optical imaging system (Caliper Life Sciences [Xenogen], Hopkinton, MA) at different time points. Five minutes prior to imaging, each mouse was given a 100μl IP injection of D-luciferin (Caliper Life Sciences [Xenogen], Hopkinton, MA) at a dose of 125mg/kg, or a 100 μl injection of 40mg/ml coelenterazine as described previously [11]. General anesthesia was then induced with 5% isoflurane (IsoSol, Medeva Pharmaceutical PA, Inc.) and the mouse was placed in the light-tight heated chamber; anesthesia was continued during the procedure with 2% isoflurane introduced via nose cone. The imaging system consists of a cooled, back-thinned charge-coupled device (CCD) camera to capture both a visible light photograph of the animal taken with light-emitting diodes and the luminescent image. After acquiring photographic images of each mouse, anterior and posterior luminescent images were acquired with 1- to 3-minute exposure times. The resulting gray scale photographic and pseudocolor luminescent images were automatically superimposed so that identification of any optical signal with location on the mouse was facilitated. Optical images were displayed and analyzed with IVIS Living Image (Caliper Life Sciences [Xenogen], Hopkinton, MA) software packages. Regions were manually drawn around the bodies of the mice to assess relative signal intensity emitted. Optical signal was expressed as photon intensity, in units of photons/second (p/s) within the region of interest (ROI).

Detection of MSC by immunohistochemistry and fluorescence

Tumors and other organs were fixed in Bouin's solution or embedded in OCT compound (Miles, Inc., Elkhart, IN) and then snap-frozen in liquid nitrogen and stored at −80°C. Frozen tissue was sectioned (6-8μm) and processed for hematoxylin-eosin, immunohistochemical staining (IHC) or direct visualization. Imaging was performed with a Zeiss Axioplan2 microscope (Carl Zeiss Inc., Thornwood, NY) equipped with a CCD camera (Hamamatsu Corp., Bridgewater, NJ) and Adobe Photoshop software (Adobe Systems Inc., San Jose, CA). *Immunohistochemistry:* Slides from frozen tissues were fixed with neutral buffered formalin (5 minutes), followed by 0.3% Hydrogen peroxide in methanol (30 minutes) to quench endogenous peroxidase. Anti- firefly luciferase IHC was preformed using a 1:500 dilution (Promega, Madison, WI). For primary antibody detection, the mouse ABC kit (Vector Labs, Burlingame, CA) was used. Peroxidase substrate was developed using either the DAB (3,3′-diaminobenzidine) or AEC (3-amino-9-ethylcarbazole) substrate kit (Vector labs, Burlingame, CA). Slides were counterstained with Hematoxylin QS (Vector labs, Burlingame, CA) and mounted using either vectamount mounting medium for DAB stained slides (Vector labs, Burlingame, CA), or with aqueous mounting medium for AEC stained slides (Scytek Laboratories, Logan, UT). For direct fluorescent visualization MSC were labeled prior to transplantation with Sp-DiI (Molecular Probes, Carlsbad, California) as described previously [24].

Statistical Analysis

Numerical data were expressed as means ± standard error. Statistical differences between the means for the different groups were evaluated with Prism 4.0 (GraphPad software) using

either the Student's T-test or analysis of variance (ANOVA), with the level of significance at $p < 0.05$.

Results

Characterization of MSC

FACS analysis demonstrated hMSC expressed high levels of CD105, CD90, CD140b, CD73, CD166, and CD44 and lower levels of CD146, in accord with accepted phenotypic markers for hMSC [44]. These cells did not express endothelial marker CD31, primitive hematopoietic marker CD34 or mature hematopoietic marker CD45 (Figure 1A). mMSC were verified to express CD44, CD106, CD140b, and Sca-1. Similarly to the human cells, mMSC were also negative for endothelial, macrophage/monocyte and pan-hematopoietic markers CD31, CD11b and CD45, respectively (Figure 1B). These patterns of expression were consistent across all MSC utilized in the following experiments. Additionally, we subjected hMSC before and after ffLuc transduction to adipogenic, osteoblastic, and chondrogenic differentiation assays. In all cases Oil red O^+, Alizarin Red S^+, and Alcian $Blue^+$ cells were detected after culture, suggesting these cells maintained their differentiation potential regardless of adenoviral transduction (Supplemental Figure 1).

Level of detection of MSC-ffLuc

Next, we demonstrated that ffLuc substrate, D-luciferin, displayed bioluminescent activity only when exposed to cells expressing ffLuc and not cells expressing renilla luciferase (rLuc). Likewise, the rLuc substrate, coelentrazine, was only active in cells expressing rLuc (Figure 1C). To determine the sensitivity of our *in vivo* detection of MSC, we injected hMSC-ffLuc beneath the skin of SCID mice. As illustrated in Figure 1D, the control animal displayed no detectable bioluminescent activity, while 300, 100, 30 and 10 cells could be detected in animals receiving SC hMSC-ffLuc.

Biodistribution of MSC in homeostatic SCID and Balb/C recipients

To follow the biodistribution of hMSC in a homeostatic host, lacking an inflamed microenvironment, hMSC-ffLuc were IV injected into SCID mice. The mice were imaged for bioluminescence detection to pinpoint hMSC-ffLuc location over time. As seen in Figure 2A, mice imaged on the day of injection (Day 1) injection showed intense signal predominantly in the lungs. The dorsal view illustrates the presence of 2 distinct hot spots of activity, which correspond to the location of two lung lobes. Bioluminescent signal decreased by 3-fold and remained localized to the lung at 3 days post-injection. However at day 5, a small population was observed exiting the lungs and appearing in the liver (Figure 2, Day 5). By 7 days post-injection, hMSC-ffLuc activity in the lung was even further reduced, and most activity was localized to the liver and spleen (Figure 2 Day 7). 10 days after injection hMSC-ffLuc activity remained in the liver and was undetectable in the lungs (Figure 2 Day 10). Photon counts of the lung region over time demonstrated a quantitative decrease from its initial peak of 21,710 +/- 9,220 p/s on day 1, becoming undetectable by day 10 (Figure 2B). Conversely, photon counts in the liver region were absent at the initial time point and slowly increased to their peak between Day 7 (2,030 +/-680 p/s) and Day 10 (2,540 +/- 1,190 p/s). After 10 days post-injection, photon counts in the liver steadily

decreased and signal was lost by Day 14 (data not shown). The presence of migrated hMSC at Day 7 was confirmed by visualizing DiI labeled hMSC in the sinus space of the liver and the lung parenchyma (Figure 2C).

In a fully immunocompetent syngeneic host, mMSC-ffLUC isolated from syngeneic Balb/C mice were similarly injected into homeostatic Balb/C mice. Interestingly, the xenograft and syngeneic models followed the same general biodistribution of localizing first to the lung and then residing in the liver, but the timeline of these events was dramatically different (Figure 2D). mMSC-ffLuc activity in the lungs peaked 1.5 hours post-injection but was not detectable by 18 hours and instead found fully distributed to the liver and spleen (Figure 2E).

hMSC localization in cutaneous wound models

Without an inflamed microenvironment, infused MSC become undetectable with time. However, in a wounded animal, the MSC localize to and remain at the site of inflammation, in this case puncture wounds and cutaneous incisions. The initial observations of MSC tropism for an acute wound were apparent in mice receiving tail vein injections (n = 5). 2.5×10^5 hMSC-ffLuc injected on day 1 show no evidence of luminescent activity in the tail, and all activity was localized to the lungs as was seen in homeostatic animals. However by day 3, signal from hMSC-ffLuc (8,910 ± 5,180 p/s) is visible at the sites of 3 needle punctures in the tail, and activity remains at day 5 (8,610 ± 1,050p/s; Figures 3A and 3C). Similar findings are evident in mice that received cutaneous incicions. Three days after surgical incision, 2.5×10^5 hMSC-ffLuc were IV injected via tail vein into the mice (Day 0). Mice were imaged 3 times a week for 2 weeks. In accord with previous findings on day 1, hMSC are found primarily in the lungs. By days 3 and 5, the hMSC-ffLuc signal in the lungs is greatly diminished while signal at the site of the sutured incision is increased (Figures 3B and 3D). At both of these time points, bioluminescence signal was significantly higher in animals with lateral incisions compared to unwounded controls that received the same MSC doses (p= 0.0001 on Day 3 and p=0.0008 on Day 5). The mice were sacrificed after two weeks and immunohistochemical analysis revealed the presence of the firefly luciferase-positive hMSC incorporated at the site of the cutaneous incisions (Figures 3E and 3F).

Systemic hMSC localization in a xenogeneic MDA-231 breast cancer model

Next, we followed systemic hMSC tropism in an inflamed, tumor microenvironment. hMSC-ffLuc localization was monitored in MDA-231 lung metastasis bearing mice. Figure 4A shows the hMSC-ffLuc on the day of injection in the lungs followed by subsequent images on days 3 and 9 showing the cells remaining in the lungs, as well as some dissemination into the liver. On day 29, the final *in vivo* image was taken before the mice were sacrificed. Quantitation of bioluminescence signal at days 9 and 29 in tumor bearing and non-tumor bearing animals which both received MSC injections revealed a statistically significant increased signal in tumor bearing animals (p=0.04 on Day 9 and p=0.02 on Day 27). The lungs, liver, spleen and kidney were removed and placed in a six-well plate. The lungs and the liver were both visually positive for tumor nodules that were also positive for hMSC-ffLuc by luminescent imaging (Figure 4B). Immunohistochemistry was performed on sections of the lung and liver tumor nodules from mice receiving MSC and mice

receiving the control PBS injection. Anti-ffLuc-positive staining is evident only in the lung and liver tumor sections of mice receiving IV hMSC-ffLuc injections (Figure 4C).

IP injected hMSC display tropism for HEY ovarian tumors

After establishing selective engraftment of systemically delivered hMSC, we evaluated hMSC tropism for HEY ovarian tumors in a model using IP injected hMSC-ffLuc. Immediately following injection, high levels of ffLuc activity were detected throughout the entire peritoneal cavity (Figure 5A). Within 3 days a unique biodistribution pattern emerged whereby hMSC-ffLUC-generated signals formed distinct punctate regions in the peritoneum. By 7 days post-injection, the overall signal was greatly reduced revealing 3-4 hot spots present in the tumor-bearing animals. In the representative animal shown in Figure 5, we observed 1 hot spot detectable only from the dorsal image in the middle of the back, 1 hot spot detected only on the ventral image at the top of the left leg, and 2 hot spots on the sides detected in both images. One region of signal (excluding the injection site) was present in control animals, corresponding to the location of the spleen. Notably, at 14 days post hMSC-ffLuc treatment, there was no detectable signal in the control animals. In contrast, the tumor-bearing HEY animals had the same hot spots as observed at day 7. Bioluminescence signal quantitated at the tumor site for HEY bearing animals was significantly greater than that of non-tumor bearing animals, as early as Day 3 ($p=0.02$). After 14 days post-MSC injection, the animals were sacrificed and the skin was removed to expose organs from the dorsal and ventral perspectives. 3 tumors were observed on the dorsal side, and 1 tumor was visible on the ventral side (identified by red arrows in Figure 5B). Bioluminescence images acquired localized hMSC-ffLuc activity specifically within these tumor locations (Figure 5B). Of importance, the anterior tumor had escaped the visceral peritoneal cavity and had established on the outside of the parietal peritoneum, yet it also displayed MSC-ffLuc activity. To confirm the localization of the hMSC-ffLuc, the tumors and organs including heart, lung, kidney, spleen, and liver were dissected and analyzed separately for bioluminescent signal. As shown in Figure 5B and 5C only the tumors displayed ffLuc activity, and all organs in both tumor-bearing and control animals were devoid of bioluminescent signal. Additionally, IHC was performed on tumor sections with anti-ffLuc to confirm the presence of hMSC-ffLuc (Figure 5D).

Systemic mMSC localization in a syngeneic, subcutaneous 4T1 breast cancer model

Finally, after observing specific tropism and selective engraftment of hMSC into the xenograft tumor microenvironment, we sought to investigate this behavior in an immunocompetent, syngeneic model. Furthermore, we investigated the tropism of systemically delivered mMSC to a subcutaneously established breast carcinoma tumor. As previously seen, the mMSC-ffLuc first localized to the lungs, but 6 days post-mMSC injection, the mMSC-ffLuc signal co-localized to areas of 4T1-rLuc activity in the subcutaneous tumors established on the legs (Figure 6A). Little ffLuc signal was seen in non-tumor bearing animals receiving mMSC-ffLuc injections, and the difference between the two groups was significant at Day 6 with a p-value of 0.0008 and at Day 12 with a p-value of 0.01. Interestingly, as the tumor grew over the next 6 days, indicated by increased rLuc signal at Day 12, the MSC-ffLuc signal increased as well (Figure 6A).

Immunohistochemistry performed at this time point on tumor sections revealed positive ffLuc staining (Figure 6B).

Discussion

We and others have shown that injected MSC engraft into tumor sites and can be utilized as effective gene delivery vehicles [1, 2, 24]. However, MSC engraftment was evidenced primarily post mortem by immunohistochemical and florescent evaluation of tissue sections. Herein, we provide direct bioluminescent evidence of *in vivo* MSC tropism for and engraftment in multiple inflammatory microenvironments over time. We suggest these consistent findings of MSC tropism and selective engraftment in multiple tumor and wound models support possible utility of exogenous MSC as biodetectors of these pathogenic conditions.

A number of studies have demonstrated that exogenously delivered MSC can be found in sites of injury [3-5]. During the wound healing process, many inflammatory factors, including chemokines, cytokines, growth factors, and extracellular matrices, may regulate the recruitment of MSC to sites of injury. Once at the injured tissue, studies have suggested that MSC aid in wound repair through differentiation into mature cell types, provision of supportive fibrovascular structures including endothelial cells and pericytes, and production of growth factors and cytokines that mediate recovery of injured cells [3-5].

Similar to the wound repair response, inflammatory cytokines, growth factors, and extracellular matrices play important roles in tumor development and progression. The stroma of malignant tumors closely resembles the granulation tissue of a healing wound [14], and the evidence suggests that solid tumors generate a wound-like environment on their periphery as they apply physical and chemical stress to neighboring tissues. Tumors can therefore be regarded as sites of tissue damage or according to Dvorak “wounds that never heal” [14].

In accord with our previous findings, human and murine MSC were readily infected with fiber-modified adenovirus and expressed the ffLuc reporter gene that was readily detectable by non-invasive imaging [11, 24, 43]. We have shown visualization of as few as 10 subcutaneously injected cells, though other reports indicate even lower levels of detection [45], and have demonstrated that larger numbers of cells result in increased bioluminescence signal. However, precise quantitation of MSC numbers in tissue embedded tumors is not possible due to differing properties of photon absorption and scattering with tissue depth. Therefore, equal bioluminescence signals from SC delivered and IV or IP delivered MSC-ffLuc will not equate to equal cell numbers and are not comparable. Therefore we can only correlate an increased or decreased photon flux to a relatively increased or decreased number of MSC present at the wounding site in the same experimental models where tumors are established and MSC are delivered by consistent routes [30].

In non-inflamed, immunocompromised SCID mice, IV injected hMSC-ffLuc systemically biodistributed to the lungs first. The hMSC remained lung-resident for 5-7 days during which time we observed diminished ffLuc signal intensity. After 5-7 days, we observed the

much decreased hMSC-ffLuc signal leaving the lungs and arising in the liver and spleen where they remained detectable until 14 days post injection. While the syngeneic, immunocompetent Balb/C model demonstrated a similar pattern of MSC migration, the period of lung residence was greatly abbreviated. In this model, nearly all ffLuc activity left the lung by 18 hours post mMSC-ffLuc IV injection. These cells were then detectable in the liver and spleen for up to 4 weeks.

In both systems we see an overall decrease of bioluminescence signal from the initial input, which is in accord with findings from other studies [46]. Only metabolically active cells will express the ffLuc reporter; thus, the decrease in bioluminescence signal is representative of a decrease in live (metabolically active) cells. Therefore we speculate that this initial decrease in photon flux is due to loss of MSC that may fail to activate critical survival and/or adhesion processes. Most groups investigating stem cell transplantation have reported overall large-scale death of transplanted cells [47, 48], and extensive effort is now being directed toward decreasing lung entrapment [46] and improving conditions for transplanted cell survival [49]. Alternatively, silencing of the ffLuc gene could occur, though little evidence of gene silencing occuring within 3-5 days after adenoviral transfection has been published. Furthermore, silencing of over 500 copies of the gene product to the point of no detection is unlikely.

Next, to investigate the biodistribution of hMSC in an archetypical, inflamed microenvironment, we generated cutaneous wounds in SCID mice and IV injected ffLuc labeled hMSC. The hMSC began to migrate to the site of the wound after 3 days and remained at the wound for the duration of the experiment. The needle puncture and sutured wound were both positive for ffLuc-hMSC generated signal after the initial residence in the lungs. Importantly, this localization was confirmed by IHC for ffLuc at the wounding site showing incorporation of the MSC into the wounded tissue microenvironment. Of interest, mice were continually monitored up to 14 days post wounding, and we observed persistent, low levels of ffLuc activity in the region of the wounded tissue even after the wound was completely healed, suggesting that the hMSC become a permanent constituent of the resolved wound site.

After evaluating MSC tropism for wounding events, we investigated this phenomenon in breast and ovarian tumor microenvironments. Irrespective of tumor type, labeled hMSC displayed tropism and selective engraftment within the site(s) of tumor development. In all cases, tumor-bearing animals displayed a statistically significant increase in ffLuc bioluminescence signal over the time courses examined when compared to their control, non-tumor bearing counterparts. These findings were consistent, though the immunocompetence of recipient mice, route of MSC administration and route of tumor establishment differed among experiments. Interestingly, many of the MSC detected by IHC in all acute insult models were found clustered together, perhaps suggesting structural formation by MSC either migrating toward each other or proliferating at the site of inflammation. In support of potential MSC proliferation at the wound site, we have previously demonstrated that MSC within the tumor microenvironment incorporate BrdU, suggesting tumor-produced mediators can stimulate MSC into proliferation [24] and subsequently contribute to tumor fibrovascular stromal components [50].

As we have previously described, MSC possess an innate tropism for sites of inflammation, including tumors and irradiated environments [2, 11, 24]. Herein, we have utilized bioluminescent imaging to visualize MSC localization to inflamed tissue microenvironments by IV and IP administration in immunocompetent and immunocompromised mice. Given the specific tropism and selective engraftment of MSC observed in all conditions, one can envision the use of labeled infused MSC as a biodetector possessing an innate tropism for inflammatory-associated chemoattractants as well as inflammatory microenvironments, which could aid in selection and monitoring progression of treatment strategies. These important findings acquired through bioluminescent imaging in the lab may readily be transitioned to the clinic through currently practiced imaging methods of positron emission tomorgraphy (PET) [40, 51, 52] and magnetic resonance imaging (MRI) [53-55] that have already been validated for visualization of transplanted MSC.

Supplementary Material

Refer to Web version on PubMed Central for supplementary material.

Acknowledgments

Supported in part by grants from the National Cancer Institute (CA-109451 and Ca-116199 for FCM, CA-55164, CA-16672, and CA-49639 for MA) and by the Paul and Mary Haas Chair in Genetics (MA). SK is supported by the Rosalie B Hite Foundation. JLD, FCM are also supported in part by grants from the Susan G Komen Breast Cancer Foundation. ELS is supported in part by Army Department of Defense (BC083397).

References

1. Nakamizo A, Marini F, Amano T, et al. Human bone marrow-derived mesenchymal stem cells in the treatment of gliomas. Cancer Res. 2005; 65:3307–3318. [PubMed: 15833864]
2. Studeny M, Marini FC, Dembinski JL, et al. Mesenchymal stem cells: potential precursors for tumor stroma and targeted-delivery vehicles for anticancer agents. J Natl Cancer Inst. 2004; 96:1593–1603. [PubMed: 15523088]
3. Sasaki M, Abe R, Fujita Y, et al. Mesenchymal stem cells are recruited into wounded skin and contribute to wound repair by transdifferentiation into multiple skin cell type. J Immunol. 2008; 180:2581–2587. [PubMed: 18250469]
4. Satake K, Lou J, Lenke LG. Migration of mesenchymal stem cells through cerebrospinal fluid into injured spinal cord tissue. Spine. 2004; 29:1971–1979. [PubMed: 15371697]
5. Neuhuber B, Timothy Himes B, Shumsky JS, et al. Axon growth and recovery of function supported by human bone marrow stromal cells in the injured spinal cord exhibit donor variations. Brain Res. 2005; 1035:73–85. [PubMed: 15713279]
6. Spaeth E, Klopp A, Dembinski J, et al. Inflammation and tumor microenvironments: defining the migratory itinerary of mesenchymal stem cells. Gene Ther. 2008
7. Murdoch C, Giannoudis A, Lewis CE. Mechanisms regulating the recruitment of macrophages into hypoxic areas of tumors and other ischemic tissues. Blood. 2004; 104:2224–2234. [PubMed: 15231578]
8. Okuyama H, Krishnamachary B, Zhou YF, et al. Expression of vascular endothelial growth factor receptor 1 in bone marrow-derived mesenchymal cells is dependent on hypoxia-inducible factor 1. J Biol Chem. 2006; 281:15554–15563. [PubMed: 16574650]
9. Chen D, Zhang Z, Wu X, et al. Distribution of intravenously grafted bone marrow mesenchymal stem cells in the viscera tissues of rats before and after cerebral ischemia. J Clin Rehab Tissue Eng Res. 2007; 11:10160–10164.
10. Spitkovsky D, Hescheler J. Adult mesenchymal stromal stem cells for therapeutic applications. Minimally Invasive Ther Allied Technol. 2008; 17:79–90.

11. Klopp AH, Spaeth EL, Dembinski JL, et al. Tumor irradiation increases the recruitment of circulating mesenchymal stem cells into the tumor microenvironment. Cancer Res. 2007; 67:11687–11695. [PubMed: 18089798]
12. Mouiseddine M, François S, Semont A, et al. Human mesenchymal stem cells home specifically to radiation-injured tissues in a non-obese diabetes/severe combined immunodeficiency mouse model. Br J Radiol. 2007; 80
13. Gorin N, Fliedner TM, Gourmelon P, et al. Consensus conference on European preparedness for haematological and other medical management of mass radiation accidents. Ann Hematol. 2006; 85:671–679. [PubMed: 16896913]
14. Dvorak HF. Tumors: wounds that do not heal. Similarities between tumor stroma generation and wound healing. N Engl J Med. 1986; 315:1650–1659. [PubMed: 3537791]
15. Wu Y, Wang J, Scott PG, et al. Bone marrow-derived stem cells in wound healing: A review. Wound Repair Regen. 2007; 15
16. Saito T, Kuang JQ, Bittira B, et al. Xenotransplant cardiac chimera: immune tolerance of adult stem cells. Ann Thorac Surg. 2002; 74:19–24. discussion 24. [PubMed: 12118756]
17. Orlic D, Kajstura J, Chimenti S, et al. Bone marrow cells regenerate infarcted myocardium. Nature. 2001; 410:701–705. [PubMed: 11287958]
18. Jackson KA, Majka SM, Wang H, et al. Regeneration of ischemic cardiac muscle and vascular endothelium by adult stem cells. J Clin Invest. 2001; 107:1395–1402. [PubMed: 11390421]
19. Bittner RE, Schofer C, Weipoltshammer K, et al. Recruitment of bone-marrow-derived cells by skeletal and cardiac muscle in adult dystrophic mdx mice. Anat Embryol (Berl). 1999; 199:391–396. [PubMed: 10221450]
20. Horwitz EM, Prockop DJ, Fitzpatrick LA, et al. Transplantability and therapeutic effects of bone marrow-derived mesenchymal cells in children with osteogenesis imperfecta. Nat Med. 1999; 5:309–313. [PubMed: 10086387]
21. Hofstetter CP, Schwarz EJ, Hess D, et al. Marrow stromal cells form guiding strands in the injured spinal cord and promote recovery. Proc Natl Acad Sci U S A. 2002; 99:2199–2204. [PubMed: 11854516]
22. Bacigalupo A. Management of acute graft-versus-host disease. Br J Haematol. 2007; 137:87–98. [PubMed: 17391488]
23. Kidd S, Spaeth E, Klopp A, et al. The (in) auspicious role of mesenchymal stromal cells in cancer: be it friend or foe. Cytotherapy. 2008; 10:657–667. [PubMed: 18985472]
24. Studeny M, Marini FC, Champlin RE, et al. Bone marrow-derived mesenchymal stem cells as vehicles for interferon-beta delivery into tumors. Cancer Res. 2002; 62:3603–3608. [PubMed: 12097260]
25. Allers C, Sierralta WD, Neubauer S, et al. Dynamic of distribution of human bone marrow-derived mesenchymal stem cells after transplantation into adult unconditioned mice. Transplantation. 2004; 78:503–508. [PubMed: 15446307]
26. Pereira RF, Halford KW, O'Hara MD, et al. Cultured adherent cells from marrow can serve as long-lasting precursor cells for bone, cartilage, and lung in irradiated mice. Proc Natl Acad Sci U S A. 1995; 92:4857–4861. [PubMed: 7761413]
27. de Wet JR, Wood KV, Helinski DR, et al. Cloning of firefly luciferase cDNA and the expression of active luciferase in Escherichia coli. Proc Natl Acad Sci U S A. 1985; 82:7870–7873. [PubMed: 3906652]
28. Contag CH, Jenkins D, Contag PR, et al. Use of reporter genes for optical measurements of neoplastic disease in vivo. Neoplasia. 2000; 2:41–52. [PubMed: 10933067]
29. Contag CH, Spilman SD, Contag PR, et al. Visualizing gene expression in living mammals using a bioluminescent reporter. Photochem Photobiol. 1997; 66:523–531. [PubMed: 9337626]
30. Contag CH, Bachmann MH. Advances in in vivo bioluminescence imaging of gene expression. Annu Rev Biomed Eng. 2002; 4:235–260. [PubMed: 12117758]
31. Sweeney TJ, Mailander V, Tucker AA, et al. Visualizing the kinetics of tumor-cell clearance in living animals. Proc Natl Acad Sci U S A. 1999; 96:12044–12049. [PubMed: 10518573]
32. Edinger M, Sweeney TJ, Tucker AA, et al. Noninvasive assessment of tumor cell proliferation in animal models. Neoplasia. 1999; 1:303–310. [PubMed: 10935484]

33. Azadniv M, Dugger K, Bowers WJ, et al. Imaging CD8+ T cell dynamics in vivo using a transgenic luciferase reporter. Int Immunol. 2007; 19:1165–1173. [PubMed: 17698980]
34. Wang X, Rosol M, Ge S, et al. Dynamic tracking of human hematopoietic stem cell engraftment using in vivo bioluminescence imaging. Blood. 2003; 102:3478–3482. [PubMed: 12946998]
35. Cao YA, Wagers AJ, Beilhack A, et al. Shifting foci of hematopoiesis during reconstitution from single stem cells. Proc Natl Acad Sci U S A. 2004; 101:221–226. [PubMed: 14688412]
36. Min JJ, Ahn Y, Moon S, et al. In vivo bioluminescence imaging of cord blood derived mesenchymal stem cell transplantation into rat myocardium. Ann Nucl Med. 2006; 20:165–170. [PubMed: 16715945]
37. van der Bogt KE, Sheikh AY, Schrepfer S, et al. Comparison of different adult stem cell types for treatment of myocardial ischemia. Circulation. 2008; 118:S121–9. [PubMed: 18824743]
38. van der Bogt KE, Schrepfer S, Yu J, et al. Comparison of transplantation of adipose tissue- and bone marrow-derived mesenchymal stem cells in the infarcted heart. Transplantation. 2009; 87:642–652. [PubMed: 19295307]
39. Togel F, Yang Y, Zhang P, et al. Bioluminescence imaging to monitor the in vivo distribution of administered mesenchymal stem cells in acute kidney injury. Am J Physiol Renal Physiol. 2008; 295:F315–21. [PubMed: 18480180]
40. Love Z, Wang F, Dennis J, et al. Imaging of mesenchymal stem cell transplant by bioluminescence and PET. J Nucl Med. 2007; 48:2011–2020. [PubMed: 18006616]
41. Hwang do W, Jang SJ, Kim YH, et al. Real-time in vivo monitoring of viable stem cells implanted on biocompatible scaffolds. Eur J Nucl Med Mol Imaging. 2008; 35:1887–1898. [PubMed: 18437378]
42. Ling X, Konopleva M, Zeng Z, et al. The novel triterpenoid C-28 methyl ester of 2-cyano-3, 12-dioxoolen-1, 9-dien-28-oic acid inhibits metastatic murine breast tumor growth through inactivation of STAT3 signaling. Cancer Res. 2007; 67:4210–4218. [PubMed: 17483332]
43. Yotnda P, Zompeta C, Heslop HE, et al. Comparison of the efficiency of transduction of leukemic cells by fiber-modified adenoviruses. Hum Gene Ther. 2004; 15:1229–1242. [PubMed: 15684699]
44. Dominici M, Le Blanc K, Mueller I, et al. Minimal criteria for defining multipotent mesenchymal stromal cells. The International Society for Cellular Therapy position statement. Cytotherapy. 2006; 8:315–317. [PubMed: 16923606]
45. Rabinovich BA, Ye Y, Etto T, et al. Visualizing fewer than 10 mouse T cells with an enhanced firefly luciferase in immunocompetent mouse models of cancer. Proc Natl Acad Sci U S A. 2008; 105:14342–14346. [PubMed: 18794521]
46. Fischer UM, Harting MT, Jimenez F, et al. Pulmonary passage is a major obstacle for intravenous stem cell delivery: the pulmonary first-pass effect. Stem Cells Dev. 2009; 18:683–692. [PubMed: 19099374]
47. Mooney DJ, Vandenburgh H. Cell delivery mechanisms for tissue repair. Cell Stem Cell. 2008; 2:205–213. [PubMed: 18371446]
48. Daley GQ, Scadden DT. Prospects for stem cell-based therapy. Cell. 2008; 132:544–548. [PubMed: 18295571]
49. Copland IB, Lord-Dufour S, Cuerquis J, et al. Improved autograft survival of mesenchymal stromal cells by plasminogen activator inhibitor 1 inhibition. Stem Cells. 2009; 27:467–477. [PubMed: 19338064]
50. Spaeth EL, Dembinski JL, Sasser AK, et al. Mesenchymal stem cell transition to tumor-associated fibroblasts contributes to fibrovascular network expansion and tumor progression. PLoS ONE. 2009; 4:e4992. [PubMed: 19352430]
51. Mayer-Kuckuk P, Doubrovin M, Bidaut L, et al. Molecular imaging reveals skeletal engraftment sites of transplanted bone marrow cells. Cell Transplant. 2006; 15:75–82. [PubMed: 16700332]
52. Hung SC, Deng WP, Yang WK, et al. Mesenchymal stem cell targeting of microscopic tumors and tumor stroma development monitored by noninvasive in vivo positron emission tomography imaging. Clin Cancer Res. 2005; 11:7749–7756. [PubMed: 16278396]
53. Bos C, Delmas Y, Desmouliere A, et al. In vivo MR imaging of intravascularly injected magnetically labeled mesenchymal stem cells in rat kidney and liver. Radiology. 2004; 233:781–789. [PubMed: 15486216]

54. Wu X, Hu J, Zhou L, et al. In vivo tracking of superparamagnetic iron oxide nanoparticle-labeled mesenchymal stem cell tropism to malignant gliomas using magnetic resonance imaging. Laboratory investigation. J Neurosurg. 2008; 108:320–329. [PubMed: 18240929]

55. Amsalem Y, Mardor Y, Feinberg MS, et al. Iron-oxide labeling and outcome of transplanted mesenchymal stem cells in the infarcted myocardium. Circulation. 2007; 116:I38–45. [PubMed: 17846324]

Abbreviations

Ad	adenovirus
α-MEM	alpha-minimal essential medium
CCD	charge-coupled device
FBS	fetal bovine serum
FDG	fluoro-deoxy-glucose
ffLuc	firefly luciferase
hMSC	human MSC
IHC	immunohistochemistry
IV	intraveneous
IP	intraperitoneal
MRI	magnetic resonance imaging
MSC	mesenchymal stem/stromal cell
MOI	multiplicity of infection
mMSC	murine MSC
PBS	phosphate buffered saline
p/s/cm^2	photons/second/centimeter^2
PET	positron emission tomography
rLuc	renilla luciferase
F/RGD	RGD-modified fiber
RPMI 1640	Roswell Park Memorial Institute medium
SCID	severe combined immune disorder mice
SC	subcutaneous

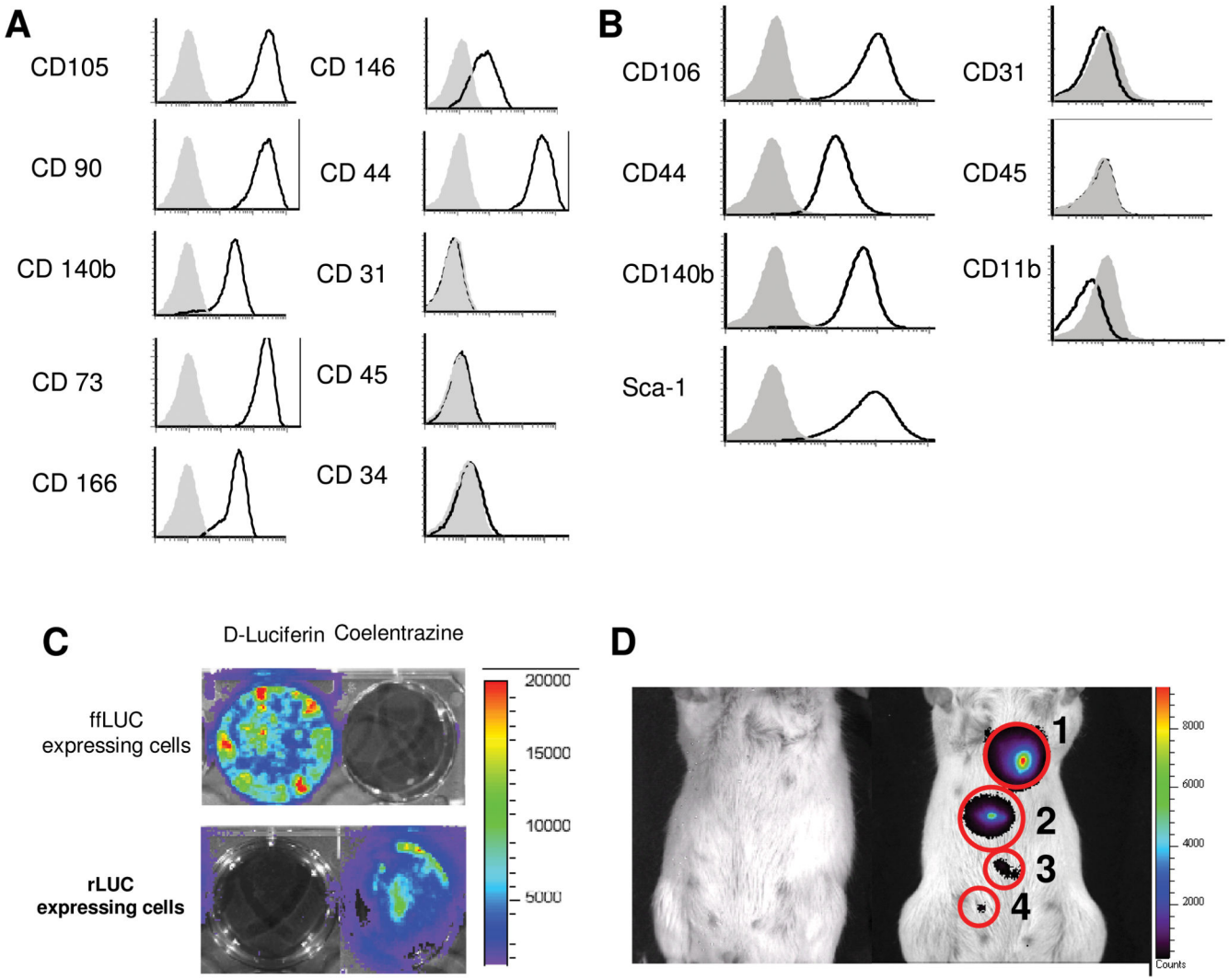

Figure 1.

MSC characterization and labeling for in vivo visualization. (A) hMSC and (B) mMSC were evaluated for phenotypic markers by flow cytometry. (C)ffLuc-expressing and rLuc-expressing cells showed specific reactivity with D-Luciferin and coelentrazine, respectively. (D) In vivo detection of MSC-ffLuc was evaluated at 0 (far left mouse), (1) 300, (2) 100, (3) 30, and (4) 10 cells per sub cutaneous injection. Increasing numbers of MSC demonstrated correlating increases in signal intensity.

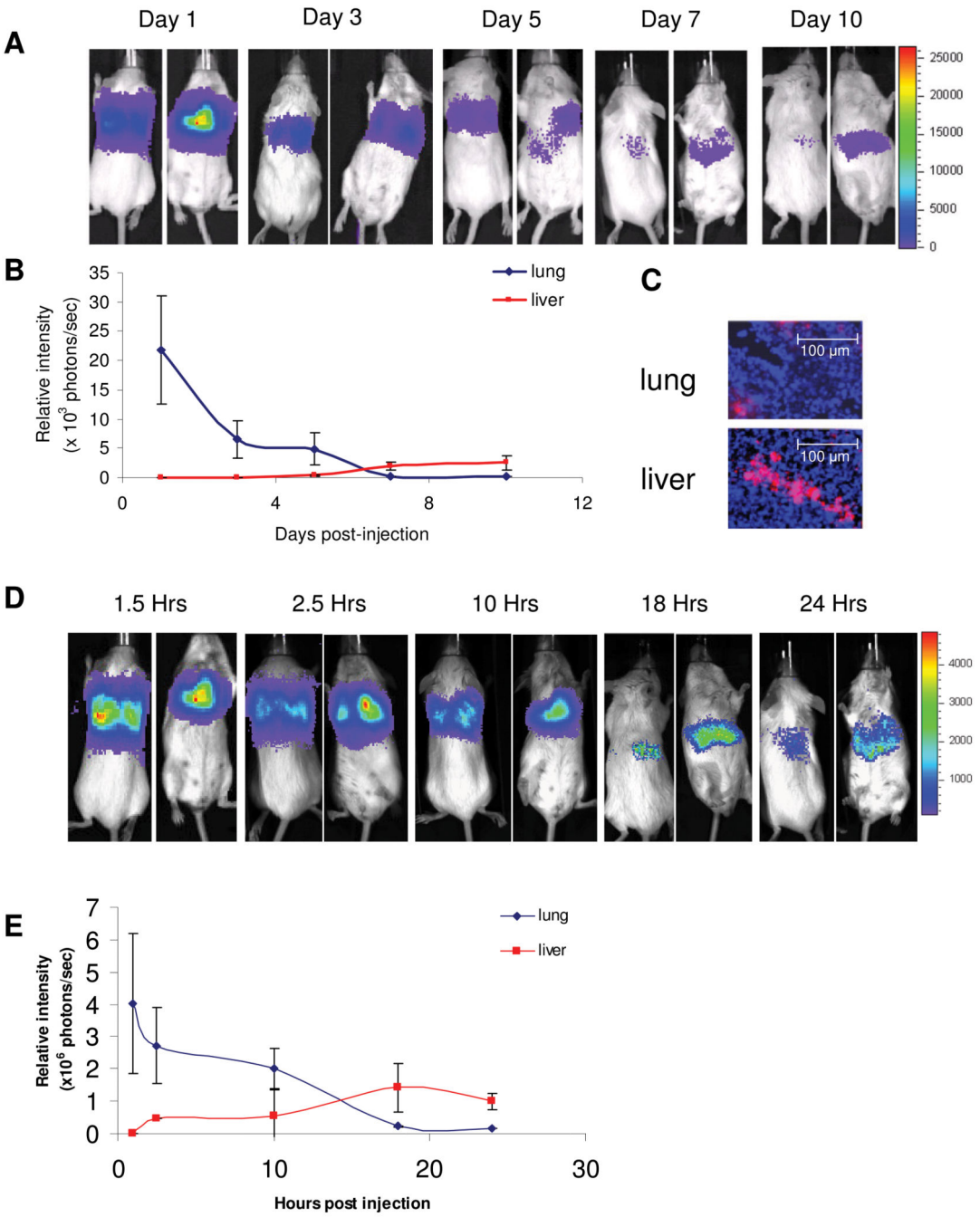

Figure 2.

Biodistribution of MSC in homeostatic animals. hMSC were IV injected into SCID mice (n=5) and (A) imaged days 1, 3, 5, 7 and 10 post-injection, showing initial localization in the lung and eventual localization in the liver and spleen by Day 10. (B) Bioluminescent signal was quantified in the lung and liver/spleen regions. (C) DiI labeled hMSC were detected in the liver and lung on Day 7 (20x magnification). In a syngeneic model, Balb/C mMSC-ffLuc were IV injected into homeostatic Balb/C mice (n=5) and (D) imaged 1.5, 2.5, 10, 18 and 24 hours post-injection. (E) The bioluminescent signal was quantified over this time

indicated initial mMSC distribution in the lung that had fully migrated to the liver/spleen by 24 hours post injection.

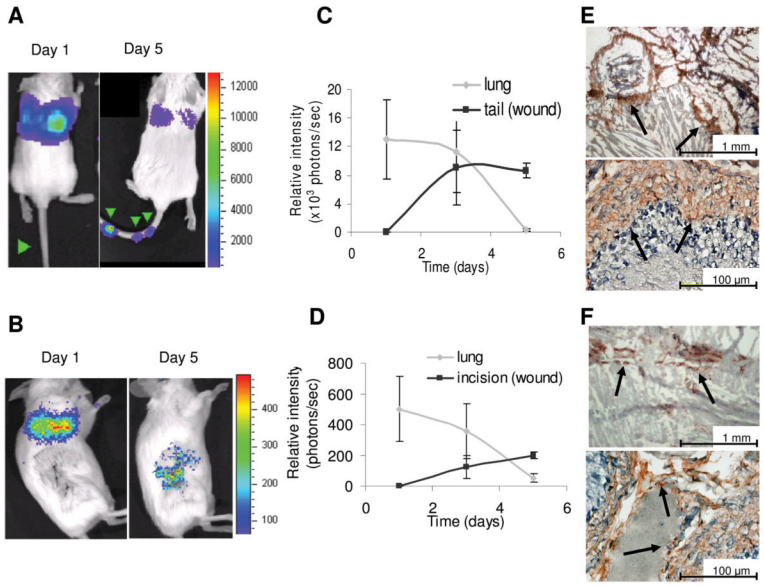

Figure 3.

hMSC co-localization with subcutaneous wound models. hMSC-ffLuc were injected immediately post needle puncture (Day 1) or 3 days post-surgical incision (Day 1). In the needle puncture model, hMSC-ffLuc were injected into SCID mice immediately post-wound infliction. Images are shown for representative animals at 1 and 5 days (A) post-needle puncture (n=5) and (B) post-lateral incision (n=3). Bioluminescent activity was quantified on days 1, 3, and 5, demonstrating a decrease in activity in the lung and concurrent increases of activity in the (C) tail wounds and (D) cutaneous incisions. IHC on sections of (E) tail and (F) wounded skin demonstrated incorporation of ff-Luc+ hMSC.

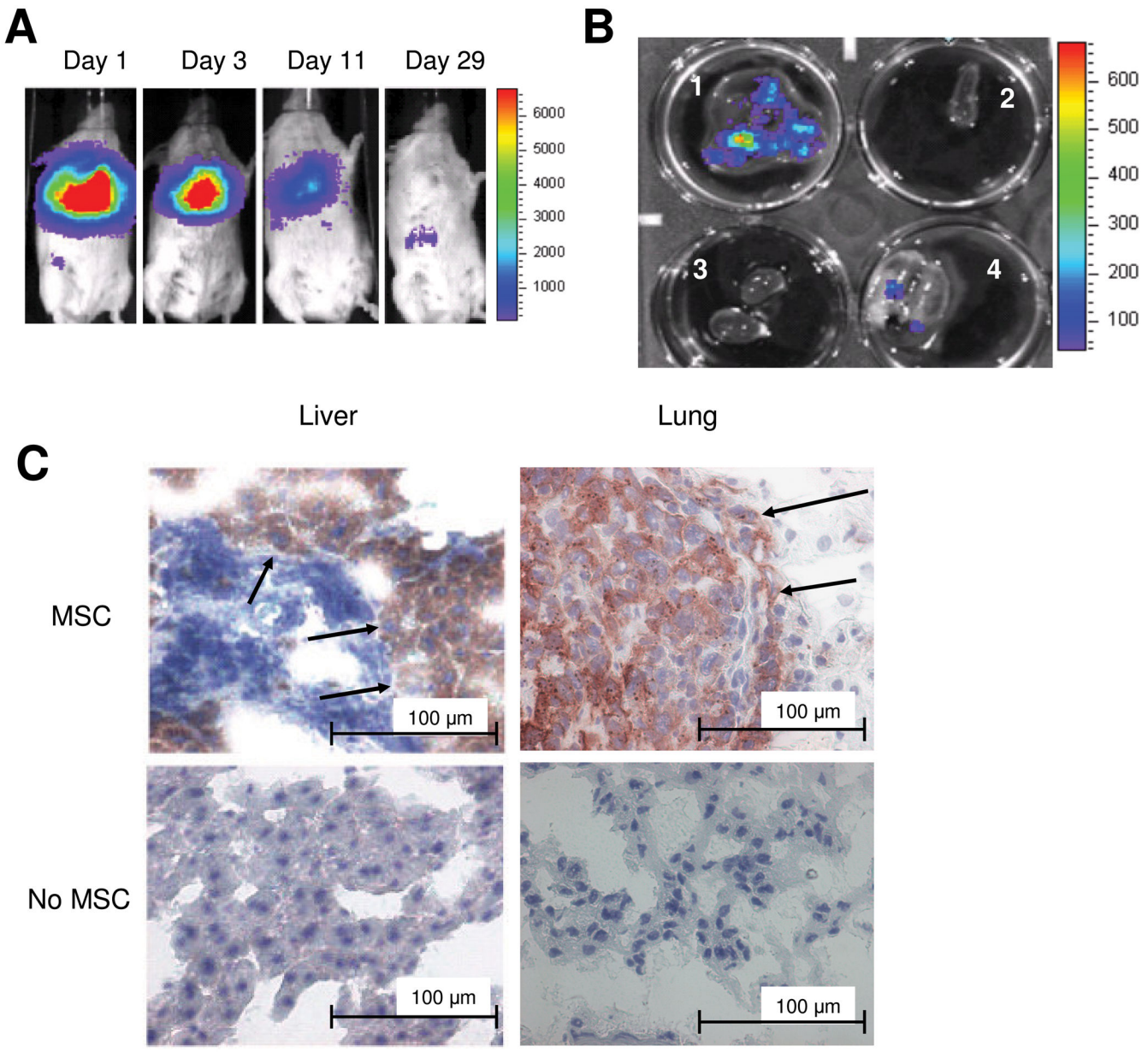

Figure 4.

hMSC co-localization with MDA-231 breast cancer in SCID mice. MDA-MB-231 cells were IV injected into SCID mice (n=5).

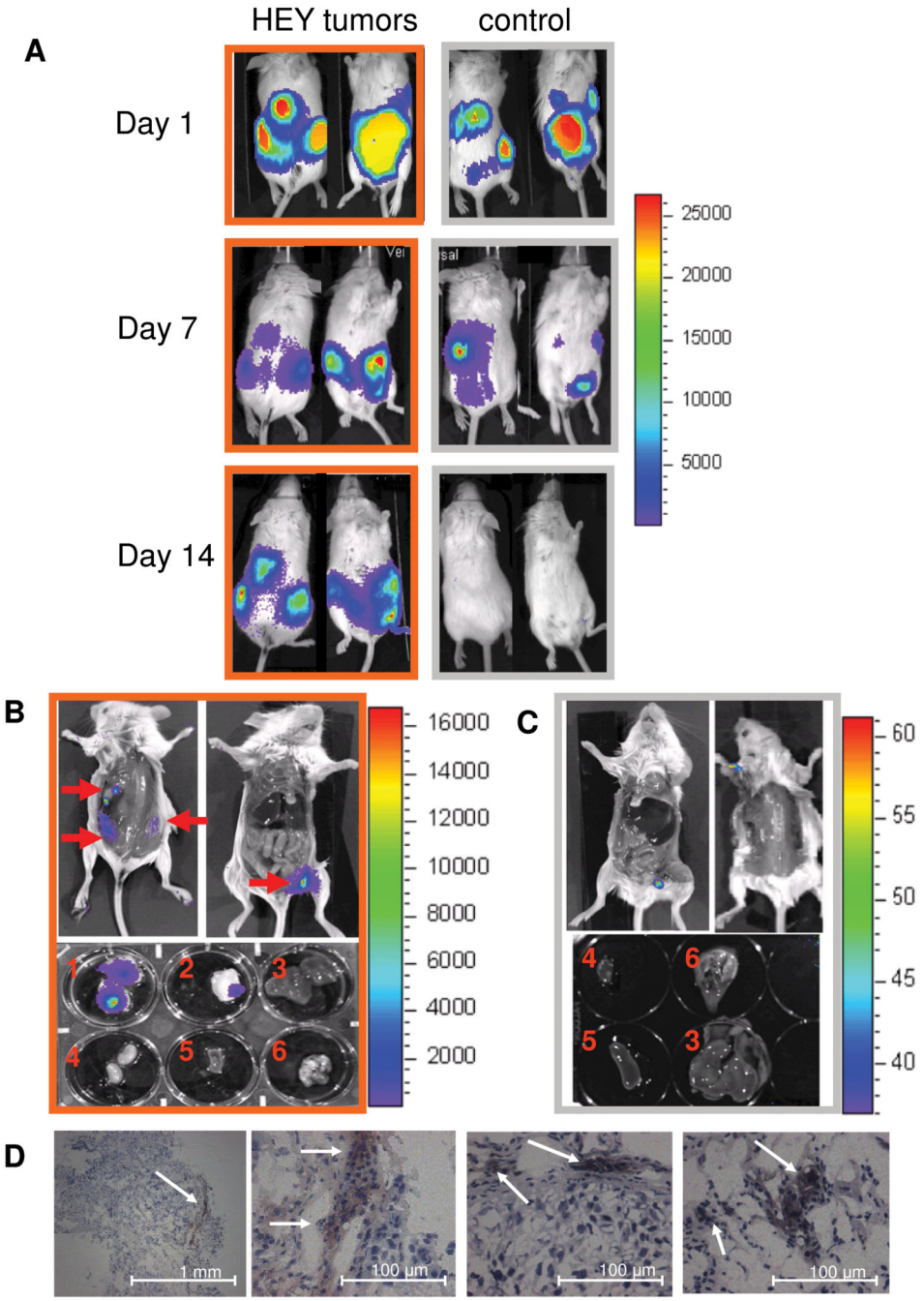

Figure 5.

MSC tropism for HEY ovarian carcinoma. SCID mice were IP injected with HEY cells (n=3; orange outline) or PBS (n=3; grey outline). 15 days later, hMSC-ffLuc were IP injected in tumor-bearing and control mice (Day 1). (A) Images were acquired at days 1, 7, and 14 indicating initial dissemination throughout the peritoneal cavity, followed by specific localization in tumor-bearing animals and disappearance in control animals. On day 14, the mice were sacrificed bioluminescent activity was localized to sites of visible tumor development in the open cavities and dissected organs [(1) ventral tumor, (2) dorsal tumor,

(3) liver, (4) kidney, (5) spleen, and (6) heart and lungs] of (B) HEY-bearing but not in (C) control mice. (D) IHC for ffLuc on tumor sections from the HEY-bearing mice confirmed the presence of hMSC (magnification as indicated).

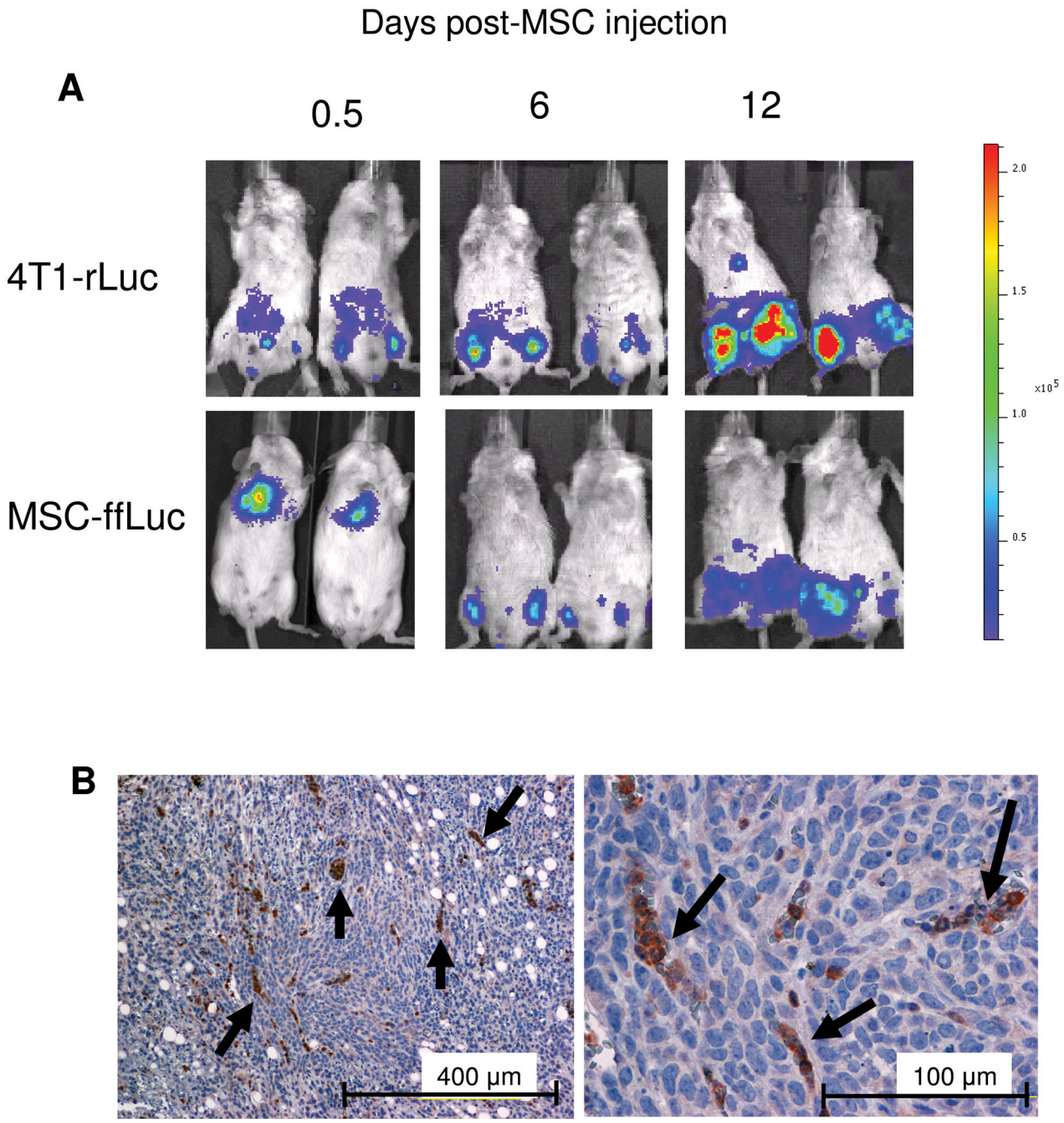

Figure 6.

mMSC co-localize with subcutaneous, syngeneic 4T1 murine breast carcinoma. 4T1 cells were subcutaneously injected into the hind limbs of Balb/C mice (n=5). 10 days post tumor establishment, mMSC-ffLuc were IV injected. (A) Mice were imaged 0.5, 6 and 12 days post mMSC-ffLuc injection for rLuc (tumor) and ffLuc (mMSC) activities, demonstrating co-localization at days 6 and 12. (B) IHC on 4T1 tumor sections revealed incorporation of ffLuc+MSC.